J|A|C|S
ARTICLES
Published on Web 02/23/2002

Electron−Nuclear Double Resonance Spectroscopic Evidence for a Hydroxo-Bridge Nucleophile Involved in Catalysis by a Dinuclear Hydrolase

Stoyan K. Smoukov,[†] Luca Quaroni,[‡] Xuedong Wang,[‡] Peter E. Doan,[†] Brian M. Hoffman,*[,†] and Lawrence Que, Jr.*[,‡]

Contribution from the Department of Chemistry, Northwestern University, Evanston, Illinois 60208, and the Department of Chemistry and Center for Metals in Biocatalysis, University of Minnesota, 207 Pleasant Street Southeast, Minneapolis, Minnesota 55455

Received August 25, 2000

Abstract: Despite the current availability of several crystal structures of purple acid phosphatases, to date there is no direct evidence for solvent-derived ligands occupying terminal positions in the active enzyme. This is of central importance, because catalysis has been shown to proceed through the direct attack on a metal-bound phosphate ester by a metal-activated solvent-derived moiety, which has been proposed to be either (i) a hydroxide ligand terminally bound to the ferric center or (ii) a bridging hydroxide. In this work we use ^{2}H Q-band (35 GHz) pulsed electron−nuclear double resonance (ENDOR) spectroscopy to identify solvent molecules coordinated to the active mixed-valence ($Fe^{3+}Fe^{2+}$) form of the dimetal center of uteroferrin (Uf), as well as to its complexes with the anions MoO_4, AsO_4, and PO_4. The solvent-derived coordination of the dinuclear center of Uf as deduced from ENDOR data includes a bridging hydroxide and a terminal water/hydroxide bound to Fe^{2+} but no terminal water/hydroxide bound to Fe^{3+}. The terminal water is lost upon anion binding while the hydroxyl bridge remains. These results are not compatible with a hydrolysis mechanism involving a terminal Fe^{3+}-bound nucleophile, but they are consistent with a mechanism that relies on the bridging hydroxide as the nucleophile.

Introduction

Hydroxo-bridged dinuclear metal clusters have emerged as the putative catalytic unit in the active sites of many dinuclear hydrolases,[1] including arginase,[2] urease,[3−5] aminopeptidase,[6,7] and a number of phosphatases.[8−17] The architecture for many of these sites is conserved even in phylogenetically unrelated enzymes,[8] prompting the suggestion that convergent evolution has acted on these proteins to promote a common but as yet not established effective catalytic mechanism. The purple acid phosphatases (PAPs) represent a subclass of these enzymes, which have been studied extensively due to the spectroscopically rich $Fe^{3+}Fe^{2+}$ or $Fe^{3+}Zn^{2+}$ sites found in their enzymatically active forms.[18−23] PAPs have been identified in bacteria, plants, and several animal tissues. In vitro they display phosphomonoesterase activity, with maximum activity in the 4−7 pH range, and broad substrate specificity, ranging from simple aryl phosphates to phosphorylated proteins. Their function in vivo is still subject to debate and has been proposed to involve fetal iron transport, control of bone resorption, and phosphate

[†] Northwestern University.
[‡] University of Minnesota.

(1) Sträter, N.; Lipscomb, W. N.; Klabunde, T.; Krebs, B. *Angew. Chem., Int. Ed. Engl.* **1996**, *35*, 2024−2055.
(2) Kanyo, Z. F.; Scolnick, L. R.; Ash, D. E.; Christianson, D. W. *Nature* **1996**, *383*, 554−557.
(3) Jabri, E.; Carr, M. B.; Hausinger, R. P.; Karplus, P. A. *Science* **1995**, *268*, 998−1004.
(4) Benini, S.; Rypniewski, W. R.; Wilson, K. S.; Miletti, S.; Ciurli, S.; Mangani, S. *Struct. Folding Des.* **1999**, *7*, 205−216.
(5) Pearson, M. A.; Michel, L. O.; Hausinger, R. P.; Karplus, P. A. *Biochemistry* **1997**, *36*, 8164−8172.
(6) Sträter, N.; Lipscomb, W. N. *Biochemistry* **1995**, *34*, 14792−14800.
(7) Lowther, W. T.; Orville, A. M.; Madden, D. T.; Lim, S.; Rich, D. H.; Matthews, B. W. *Biochemistry* **1999**, *38*, 7678−7688.
(8) Lohse, D. L.; Denu, J. M.; Dixon, J. E. *Structure* **1995**, *3*, 987−990.
(9) Egloff, M.-P.; Cohen, P. T. W.; Reinemer, P.; Barford, D. *J. Mol. Biol.* **1995**, *254*, 942−959.
(10) Kissinger, C. R.; Parge, H. E.; Knighton, D. R.; Lewis, C. T.; Pelletier, L. A.; Tempczyk, A.; Kalish, V. J.; Tucker, K. D.; Showalter, R. E.; Moomaw, E. W. *Nature* **1995**, *378*, 641−644.
(11) Goldberg, J.; Huang, H.; Kwon, Y.; Greengard, P.; Nairn, A. C.; Kuriyan, J. *Nature* **1995**, *376*, 745−753.
(12) Sträter, N.; Klabunde, T.; Tucker, P.; Witzel, H.; Krebs, B. *Science* **1995**, *268*, 1489−1492.
(13) Klabunde, T.; Sträter, N.; Fröhlich, R.; Witzel, H.; Krebs, B. *J. Mol. Biol.* **1996**, *259*, 737−748.
(14) Uppenberg, J.; Lindqvist, F.; Svensson, C.; Ek-Rylander, B.; Andersson, G. *J. Mol. Biol.* **1999**, *290*, 201−211.
(15) Lindqvist, Y.; Johansson, E.; Kaija, H.; Vihko, P.; Schneider, G. *J. Mol. Biol.* **1999**, *291*, 135−147.
(16) Guddat, L. W.; McAlpine, A. S.; Hume, D.; Hamilton, S.; Jersey, J. d.; Martin, J. L. *Structure* **1999**, *7*, 757−767.
(17) Voegtli, W. C.; White, D. J.; Reiter, N. J.; Rusnak, F.; Rosenzweig, A. C. *Biochemistry* **2000**, *39*, 15365−15374.
(18) Klabunde, T.; Krebs, B. *Struct. Bonding (Berlin)* **1997**, *89*, 177−198.
(19) Gehring, S.; Fleischhauer, P.; Behlendorf, M.; Hüber, M.; Lorösch, J.; Haase, W.; Dietrich, M.; Witzel, H.; Löcke, R.; Krebs, B. *Inorg. Chim. Acta* **1996**, *252*, 13−17.
(20) Day, E. P.; David, S. S.; Peterson, J.; Dunham, W. R.; Bonvoisin, J. J.; Sands, R. H.; Que, L., Jr. *J. Biol. Chem* **1988**, *263*, 15561−15567.
(21) Averill, B. A.; Davis, J. C.; Burman, S.; Zirino, T.; Sanders-Loehr, J.; Loehr, T. M.; Sage, J. T.; Debrunner, P. C. *J. Am. Chem. Soc.* **1987**, *109*, 3760−3767.
(22) Yang, Y.-S.; McCormick, J. M.; Solomon, E. I. *J. Am. Chem. Soc.* **1997**, *119*, 11832−11842.
(23) David, S. S.; Que, L., Jr. *J. Am. Chem. Soc.* **1990**, *112*, 6455−6463.

10.1021/ja003169l CCC: $22.00

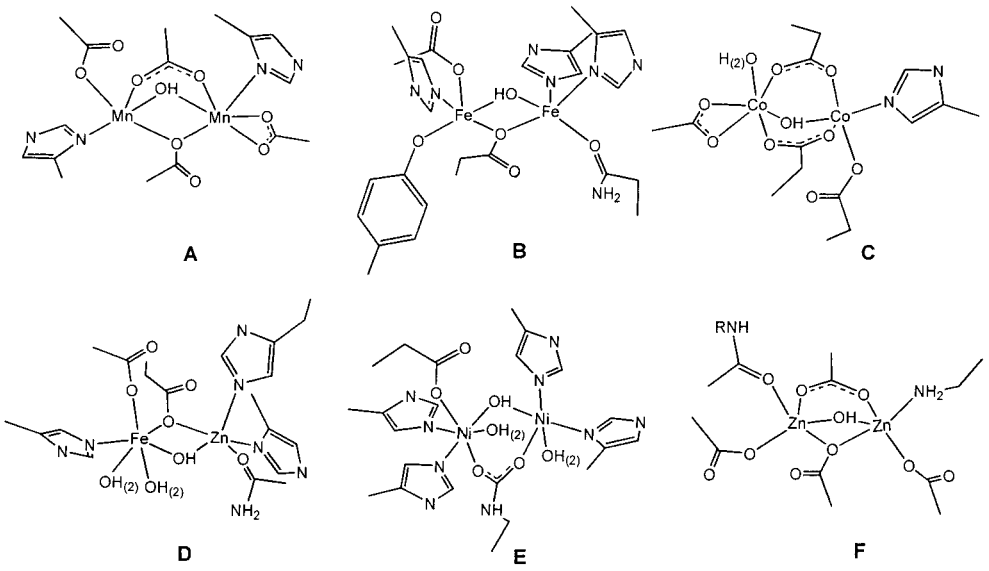

Figure 1. Metal clusters of some hydrolases displaying a hydroxo-bridged dinuclear metal site. A, arginase (1cev); B, purple acid phosphatase (1ute); C, methionine aminopeptidase (2mat); D, calcineurin (1aui); E, urease (1fwj); F, leucine aminopeptidase (1lam). The structures have been derived from the PDB files indicated in parentheses.

homeostasis in plants.[24,25] Crystal structures of PAPs show that seven conserved protein residues, including a monodentate bridging carboxylate, occupy eight coordination sites on the two metals, leaving four possible sites for exogenous ligands (Figure 1).[12−16] The presence of a hydroxo bridge occupying two of the exogenous ligand sites has been proposed on the basis of spectroscopic and magnetic measurements of the active mixed-valence $Fe^{3+}Fe^{2+}$ enzyme[21−23] and corroborated by the crystal structures of the inactive $Fe^{3+}Fe^{3+}$ form of two mammalian enzymes.[15,16] Crystal structures also show that the two remaining terminal coordination sites can be occupied by a bidentate phosphate or tungstate.[13] However, to date there is no direct evidence for solvent-derived ligands occupying these terminal positions in the active enzyme. This is of central importance for an understanding of the catalytic mechanism.

Enzymatic hydrolysis of phosphate monoesters is generally believed to occur via a nucleophilic substitution mechanism.[1] The nucleophile adds to the tetrahedral phosphorus atom on the opposite side of the leaving group, to give a pentacoordinate trigonal bipyramidal intermediate or transition state where the incoming nucleophile and the leaving group are lined up to occupy the axial positions. In metallophosphatases, the metal has been shown to have multiple functions, including activation of the nucleophile, activation of the phosphate ester substrate, control of their reciprocal orientation, and stabilization of the pentacoordinate transition state. Phosphate hydrolysis by the PAP from bovine spleen occurs with full inversion of configuration at the phosphorus center.[26] Such stereospecificity is consistent with a mechanism involving the direct attack of a water or hydroxide nucleophile on the phosphate ester, without the formation of a phosphoenzyme intermediate. This is confirmed by the failure to observe burst kinetics in PAPs,[27] as

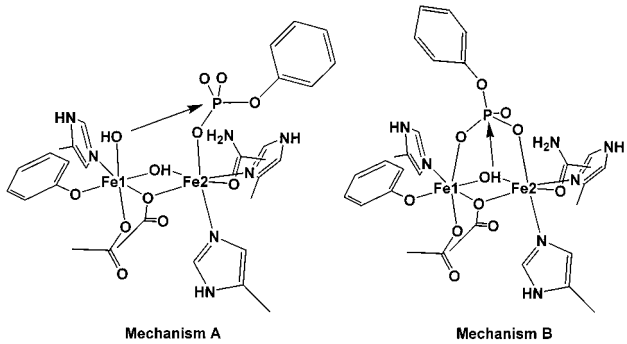

Figure 2. Proposed mechanisms for the hydrolysis of a phosphate monoester by PAPs, involving either a terminal (mechanism A) or a bridging (mechanism B) nucleophile.

found for alkaline phosphatase and other hydrolases that form a covalent intermediate.[28] The low pH range at which PAPs display maximal activity (pH 4−7) requires that the moiety initiating the P−O bond cleavage event be nucleophilically activated, probably through direct coordination to a metal center or hydrogen-bonding contact to the same.

To date the nucleophile has eluded identification, not least because of the inability of X-ray crystallography to describe the complete coordination sphere of the metal centers in the active enzyme. Two different proposals assign it to either (i) a hydroxide ligand terminally bound to the ferric center[13,29−31] or (ii) a bridging hydroxide (Figure 2).[32,33]

The ligand arrangement proposed in mechanism A (Figure 2) models the one believed to occur in the hydrolysis of the phosphorylated intermediate of alkaline phosphatase.[13] In the latter, a phosphoserine coordinated to one Zn^{2+} cation of the dinuclear center via one of its phosphoryl oxygen atoms is

(24) Roberts, R. M.; Bazer, F. W. *BioEssays* **1984**, *1*, 8−11.
(25) Oddie, G. W.; Schenk, G.; Angel, N. Z.; Walsh, N.; Guddat, L. W.; De Jersey, J.; Cassady, A. I.; Hamilton, S. E.; Hume, D. A. *Bone (N. Y.)* **2000**, *27*, 575−584.
(26) Mueller, E. G.; Crowder, M. W.; Averill, B. A.; Knowles, J. R. *J. Am. Chem. Soc.* **1993**, *115*, 2974−2975.
(27) Merkx, M.; Pinkse, M. W. H.; Averill, B. A. *Biochemistry* **1999**, *38*, 9914−9925.
(28) Coleman, J. E. *Annu. Rev. Biophys. Biomol. Struct.* **1992**, *21*, 441−483.
(29) Aquino, M. A. S.; Lim, J.-S.; Sykes, A. G. *J. Chem. Soc., Dalton Trans.* **1994**, 429−436.
(30) Twitchett, M. B.; Sykes, A. G. *Eur. J. Inorg. Chem.* **1999**, 2105−2115.
(31) Dietrich, M.; Münstermann, D.; Suerbaum, H.; Witzel, H. *Eur. J. Biochem.* **1991**, *199*, 105−113.
(32) Wang, X.; Ho, R. Y. N.; Whiting, A. K.; Que, L., Jr. *J. Am. Chem. Soc.* **1999**, *121*, 9235−9236.
(33) Kimura, E. *Curr. Opin. Chem. Biol.* **2000**, *4*, 207−213.

attacked by a hydroxide ion terminally bound to the opposite Zn^{2+} center, oriented to effect an in-line attack on the phosphorus atom and displace the serine leaving group.[28] This picture is also supported by the structure observed for the sulfate complex of a diferric PAP,[15] where the tetrahedral oxoanion is terminally coordinated to Fe_2, while a hydroxide ion is coordinated to Fe_1 (Figure 2). In a variant of this mechanism, the terminal hydroxide ligand coordinated to Fe^{3+} does not act as the nucleophile directly. Instead it acts as a base and deprotonates a water molecule in the substrate pocket that would in turn be the nucleophile responsible for attack on the metal-bound phosphate ester.[27,34]

The ligand arrangement in mechanism B (Figure 2) is based on the notion that the complex of uteroferrin with phosphate has a structure similar to that of the enzyme−substrate complex. This mechanism is based on the observation that phosphate is a competitive inhibitor of PAPs and is expected to bind to the substrate-binding pocket with similar interactions. Crystallographic and extended X-ray absorption fine structure (EXAFS) spectroscopic studies of the phosphate complex of several PAPs agree in showing the phosphate ion bound to both metal ions with a bidentate bridging geometry.[13,16,35,36] The same coordination geometry has been reported or proposed for other bound tetrahedral oxoanions, all of them capable of inhibiting activity, including molybdate, tungstate, and arsenate.

In this work we use ^2H Q-band pulsed electron−nuclear double resonance (ENDOR) spectroscopy to identify solvent-derived moieties coordinated to the active mixed-valence Fe^{3+}-Fe^{2+} form of uteroferrin (Uf) and its complexes with MoO_4, AsO_4, and PO_4. The resulting structural information is compatible with only one of the two proposed mechanisms for phosphate ester hydrolysis.

Materials and Methods

Uteroferrin was isolated and purified from the uteri of gilts treated with β-estradiol-17-valerate according to the published procedure.[37] ENDOR samples were prepared in 10−30% glycerol or ethylene glycol. The anion complexes were prepared by adding a buffered solution of the anion in water/glycerol or water/ethylene glycol to the protein under gentle stirring. The AsO_4 and PO_4 complexes are air-sensitive and were prepared under an argon atmosphere. The samples in D_2O were prepared by repeated concentration of the protein solution in Centricon (Amicon, Beverly, MA) tubes (10 kDa cutoff) and dilution with D_2O buffer of the desired pD. D_2O buffer was prepared by drying an aliquot of buffer solution under vacuum and resuspending the salt deposit in the corresponding volume of D_2O. The pD of the deuterated buffer was then adjusted to the desired value with glacial acetic acid (acetate buffers) or concentrated HCl/NaOD [(3-morpholinopropanesulfonic acid (MOPS) buffer]. The buffers used were 0.1 M sodium acetate buffer, pH/pD 4.9, containing 0.2 M NaCl, and 0.1 M MOPS buffer, pH/pD 7.0, containing 0.2 M NaCl. Anion solutions were prepared by dissolving the appropriate salt in H_2O/D_2O buffer and adjusting the pH/pD of the solution. $(NH_4)_2MoO_4$ and $Na_2HAsO_4{\cdot}7H_2O$ were analytical-grade reagents from Mallinckrodt (Parks, KY). NaCl was ACS reagent-grade from Fisher. $Na_2HPO_4{\cdot}7H_2O$, $NaH_2PO_4{\cdot}H_2O$, and MOPS were acquired from Sigma. Ethylene glycol-d_6 was bought from Cambridge Isotope Laboratories (Cambridge, MA). Glycerol-d_3 was prepared by repeated dilution of glycerol in D_2O, followed by vacuum-drying.

Previously described 35 GHz pulsed ENDOR instrumentation[38] and procedures were applied. Spectra were recorded at 2 K. The Mims three-pulse,[39,40] Re-Mims four-pulse,[41] and Davies[42] three-pulse techniques were used to collect pulsed ENDOR spectra. The magnet power supply on the 35 GHz pulsed ENDOR instrument permitted us to collect data up to fields of ~16 500 G, corresponding to $g \sim 1.52$; thus, only the extreme high-field edge of the electron paramagnetic resonance (EPR) envelope of the Uf·molybdate complex was inaccessible for ENDOR measurement (see below).

The Mims technique utilizes a three-pulse electron spin−echo sequence ($t_p-\tau-t_p-T-t_p-\tau-$echo), where t_p is the microwave pulse width; the Rf pulse is inserted during the interval, T.[39,40] This technique has a response R that depends on the product $A\tau$, where τ is the time between the first and second microwave pulse, according to

$$R \sim [1 - \cos(2\pi A\tau)] \qquad (1)$$

This function has zeroes, corresponding to minima in the ENDOR response (hyperfine "suppression holes"), at $A\tau = n$, $n = 0, 1, ...$, and maxima at $A\tau = (2n + 1)/2$, $n = 0, 1, ...$ For instrumental dead-time reasons, the shortest τ value usually achievable on our 35 GHz pulsed spectrometer is 300−350 ns. When shorter values of τ were desirable, we employed the Re-Mims four-pulse[41] ENDOR technique, which permits the use of much shorter values of τ. This technique also displays the suppression holes characteristic of the Mims sequence but makes the choice of τ independent of the instrumental deadtime.

The Davies technique signal intensity depends not on the product $A\tau$ but on the product At_p and is most useful for nuclei with large hyperfine couplings.

The ENDOR pattern for a single orientation of a nucleus with spin I consists of two branches of $2I$ lines each, with first-order frequencies:

$$\nu_{\pm}^{(m)} = |\nu_N \pm (A/2) + {}^3/_2P(2m - 1)| \qquad I \geq m \geq (-I + 1) \quad (2)$$

where A and P are the orientation-dependent hyperfine and quadrupole couplings. All ENDOR signals displayed here, except the ones for ^{14}N, arise from nuclei with Larmor frequencies $\nu > A/2$, in which case the two branches are centered at the Larmor frequency and separated by the hyperfine interaction A; for the nuclei with $I > {}^1/_2$, namely, ^2H ($I = 1$), ^{14}N ($I = 1$), and ^{95}Mo ($I = {}^5/_2$), each branch is further split or broadened by the nuclear quadrupole interaction. The ^{14}N signals, on the other hand, are centered at $A/2$ and the two branches are separated by twice the ^{14}N Larmor frequency. Techniques for simulating frozen-solution spectra and for analyzing two-dimensional field-frequency plots composed of multiple ENDOR spectra taken across the EPR envelope of a paramagnetic center in a frozen solution have been published.[43] Simulations were performed with the GENSIM program,[44] modified to include Mims suppression effects.

Results

The active form of uteroferrin possesses an antiferromagnetically coupled $S_1 = {}^5/_2$, $S_2 = 2$ diiron center with $S_{tot} = {}^1/_2$. The protein gives a broad and rhombic EPR signal from the $S = {}^1/_2$ diiron center that is detectable only at low temperatures[20,23] (**g** tensor given in Table 1). The observed g anisotropy and the

(34) Merkx, M.; Averill, B. A. *J. Am. Chem. Soc.* **1999**, *121*, 6683−6689.
(35) Wang, X.; Que, L., Jr. *Biochemistry* **1998**, *37*, 7813−7821.
(36) True, A. E.; Scarrow, R. C.; Randall, C. R.; Holz, R. C.; Que, L., Jr. *J. Am. Chem. Soc.* **1993**, *115*, 4246−4255.
(37) Pyrz, J. W.; Sage, J. T.; Debrunner, P. G.; Que, L., Jr. *J. Biol. Chem.* **1986**, *261*, 11015−11020.
(38) Davoust, C. E.; Doan, P. E.; Hoffman, B. M. *J. Magn. Reson.* **1996**, *119*, 38−44.
(39) Mims, W. B. *Proc. R. Soc. London* **1965**, *283*, 452−457.
(40) Gemperle, C.; Schweiger, A. *Chem. Rev.* **1991**, *91*, 1481−1505.
(41) Doan, P. E.; Hoffman, B. M. *Chem. Phys. Lett.* **1997**, *269*, 208−214.
(42) Davies, E. R. *Phys. Lett.* **1974**, *47A*, 1−2.
(43) Hoffman, B. M.; DeRose, V. J.; Doan, P. E.; Gurbiel, R. J.; Houseman, A. L. P.; Telser, J. In *Biological Magnetic Resonance*; Berliner, L. J., Reuben, J., Eds.; Plenum Press: New York and London, 1993; Vol. 13, pp 151−218.
(44) Available currently by request from Peter Doan: e-mail ped131@nwu.edu.

Table 1. **g** Tensors of $Fe^{3+}Fe^{2+}$Uf and Its Complexes with Tetraoxo Anions

Uf complex name	**g**-tensor	ref
$Fe^{3+}Fe^{2+}$Uf	[1.96, 1.74, 1.56]	20
$Fe^{3+}Fe^{2+}$Uf·MoO_4	[1.97, 1.52, 1.52]	20
$Fe^{3+}Fe^{2+}$Uf·AsO_4	[1.92, 1.58, 1.41−1.44]	23
$Fe^{3+}Fe^{2+}$Uf·PO_4	[2.27, 1.51, 1.06]	20

temperature dependence of the EPR spectrum both suggest close proximity of excited states, indicating a weak antiferromagnetic coupling. Indeed, magnetic susceptibility measurements[20] have determined that $J = 20$ cm^{-1} ($H = JS_1 \cdot S_2$). The addition of tetraoxo anions to uteroferrin significantly changes its **g** tensor (Table 1). These changes are symptomatic of the weakening of the antiferromagnetic interaction; in fact, magnetic susceptibility measurements[20] show that for the PO_4 complex J decreases to 6 cm^{-1}.

^{14}N, ^{95}Mo, ^{75}As ENDOR. Figure 3A presents Davies and Mims pulsed ENDOR spectra of FeFeUf·$^{95}MoO_4$ collected at $g_2 = 1.52$ in the frequency region, 1−25 MHz. It shows the ν_+ peak from the histidyl nitrogen bound to Fe^{3+} (^{14}N1), centered at $\nu_+ = A/2 + \nu_N = 14.9$ MHz ($\nu_N = 5.05$ MHz), giving $A = 19.7$ MHz; the quadrupole interaction is not resolved. The coupling for N1 is significantly smaller than that for the corresponding N in MMO (e.g., $A = [22, 22, 29.5]$, $A_{obs}(g_2) = 25$ MHz).[45] In the lower frequency range, ≤7−10 MHz, the spectrum has additional intensity from the nitrogens bound to Fe^{2+}, which have a much smaller hyperfine coupling (^{14}N2). Similar ^{14}N signals are seen in the other anion complexes of Uf as well and will not be discussed further.

The spectrum of FeFeUf·$^{95}MoO_4$ reveals a pair of ENDOR peaks, centered at $\nu(^{95}\text{Mo}) = 4.57$ MHz. These have minimal intensity in the sample with natural-abundance Mo (^{95,97}Mo = 25.5%), and thus are assigned as the ν_+, ν_- branches of bound ^{95}Mo molybdate, with a splitting of A(Mo) = 1.8 MHz. In principle, the two branches of a ^{95}Mo ($I = {}^5/_2$) ENDOR signal should be split into five lines by the quadrupole interaction (see Materials and Methods section above). We interpret the absence of such splitting to mean that the quadrupole coupling constant is negligible, as would be the case for an ideally tetrahedral molybdate ion. We note that a simple doublet also would arise in the opposite extreme. The quadrupole coupling could be so large that all nuclear transitions are broadened into unobservability, except for the pair of peaks associated with the ^{95}Mo nuclear spin transition $|I, m_I\rangle = |{}^5/_2, \pm{}^1/_2\rangle$, which has no quadrupole terms associated with it in first order. However, this situation is unlikely, given the inherent symmetry of the molybdate ion, and it is ruled out by the fact that the doublet is, indeed, centered at the ^{95}Mo Larmor frequency; as we have observed with the ENDOR spectra of ^{17}O ($I = {}^5/_2$),[46] when the quadrupole interaction is appreciable, second-order terms shift the $\nu_\pm$ branches relative to $\nu(^{95}\text{Mo})$.

This ^{95}Mo signal could be collected over the EPR envelope through a combination of Davies and Mims pulsed ENDOR spectra (Figure 3B). At the lower g values (higher fields) the Mo features show well with the Davies protocol. At higher g values they become indistinct against the ^{14}N background in Davies ENDOR but are well resolved in Mims spectra, although the Mims suppression holes (eq 1) cause some peak distortion and result in an apparent decrease in the hyperfine splitting. As shown in Figure 3B, the center of the ^{95}Mo doublet tracks with the ^{95}Mo Larmor frequency as required; the splitting of the doublet remains essentially invariant, indicating that the hyperfine coupling is primarily isotropic, with A_{iso}(Mo) ≈1.8 MHz. Such an interaction requires a through-bond linkage to the metal

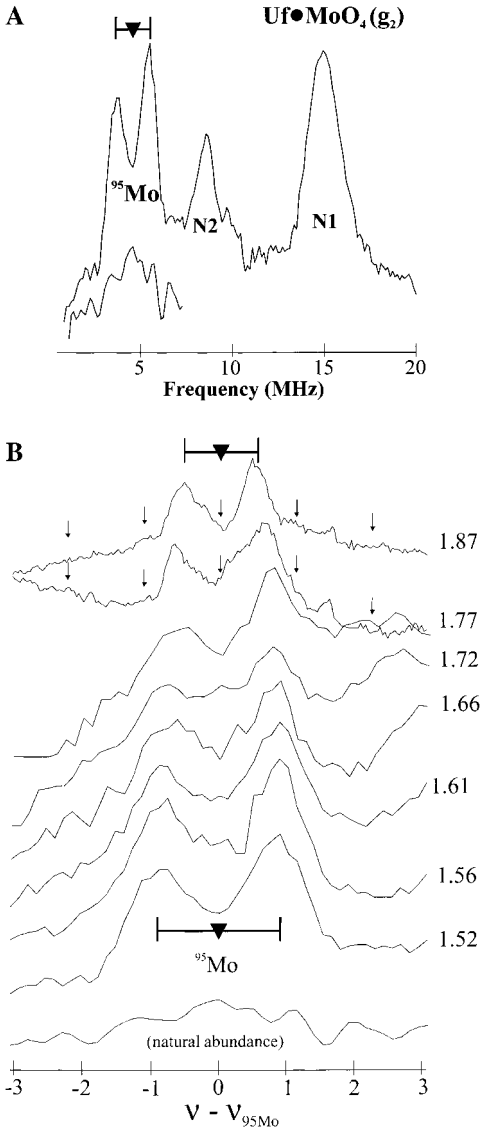

Figure 3. (**A**, **top panel**) ^{14}N and ^{95}Mo Davies pulsed ENDOR spectrum at $g_2 = 1.52$ of Uf + MoO_4 in H_2O at pH = 4.9. (Upper trace**)** Sample with $^{95}MoO_4$, 34.849 GHz MW frequency, $\tau = 1106$ ns; pulse lengths = 200, 100, and 200 ns, with 100 μs Rf pulse between pulses 2 and 3, repetition time 4 ms, 250 shots per point per scan, two scans. **(**Lower trace**)** Background sample with natural abundance MoO_4, 34.741 GHz MW frequency, $\tau = 1106$ ns; pulse lengths = 200, 100, and 200 ns, with 100 μs Rf pulse between pulses 2 and 3, repetition time 10 ms, 50 shots per point per scan, five scans. (**B**, **bottom panel**) Field-dependent ^{95}Mo Mims and Davies pulsed ENDOR spectra of Uf + MoO_4 in H_2O buffer at pH = 4.9. Conditions for the top two spectra: Mims three-pulse sequence, pulse lengths $t_p = 52$ ns; 60 μs Rf pulse between pulses 2 and 3: $\tau = 452$ ns; 34.822 GHz MW frequency, repetition time 10 ms; 100 shots per point per scan, ($g = 1.87$) two scans, ($g = 1.77$) three scans. Conditions for the rest of the spectra: 34.849 GHz MW frequency, Davies three-pulse sequence, $\tau = 1106$ ns; pulse lengths = 200, 100, and 200 ns, with 100 μs Rf pulse between pulses 2 and 3, repetition time 4 ms, 250 shots per point per scan, ($g = 1.778$) three scans, ($g = 1.717$) three scans, ($g = 1.660$) three scans, ($g = 1.606$) two scans, ($g = 1.556$) one scan, ($g = 1.518$) two scans.

(45) DeRose, V. J.; Liu, K. E.; Lippard, S. J.; Hoffman, B. M. *J. Am. Chem. Soc.* **1996**, *118*, 121−134.
(46) Jin, H.; Turner, I. M., Jr.; Nelson, M. J.; Gurbiel, R. J.; Doan, P. E.; Hoffman, B. M. *J. Am. Chem. Soc.* **1993**, *115*, 5290−5291.

center and confirms that $^{95}MoO_4$ is bound to the mixed-valence diiron center in the solution enzyme. A previous X-band CW ENDOR investigation[47] detected ^{95}Mo signals by ENDOR and electron spin−echo envelope modulation (ESEEM) spectroscopy at one field ($g\perp$).

Similar experiments with FeFeUf·$^{75}AsO_4$ showed the signals from N1 and N2, but nothing that could be attributed to ^{75}As (100% abundance), despite the fact that the large change in the EPR **g** tensor in the presence of arsenate confirms that a complex is formed. A possible explanation is quadrupole broadening. The quadrupole moment for ^{75}As is roughly 15-fold larger than that of ^{95}Mo, and even in a nearly tetrahedral environment its interaction could make detection difficult. We were not able to observe ^{31}P signals from FeFeUf·PO_4 either, even though the spin $^1/_2$ of the ^{31}P nucleus is in 100% abundance and its high Larmor frequency would be expected to make it responsive to ENDOR detection. However, in our experience, ^{31}P signals have been much harder to detect than ^{1}H ones; even in the cases where we have detected them, they have been much less intense than those from ^{1}H. Nonetheless, there is direct evidence from EPR line broadening in the analogous FeZnUf·$P^{17}O_4$ complex that phosphate binds to the trivalent Fe ion.[23]

^{1,2}H ENDOR. Figure 4 presents Mims ^{2}H Q-band ENDOR spectra taken at g_2 for Uf in D_2O buffers at pD 7 and pD 4.9, along with g_2 spectra of the Uf·MoO_4, Uf·AsO_4, and Uf·PO_4 complexes at pD 4.9; it includes both the complete spectra (panel A) and expansions of the central region (panel B). For reference, the figures include the corresponding ^{1}H frequency scale. Signals from three resolved deuterons will be discussed successively.

Deuteron 1. Considering first the wide scans of Figure 4A, the top four spectra show a well-defined doublet of broad peaks at $\nu_{+/-} \sim \pm(1.5-2)$ MHz, corresponding to a hyperfine coupling $A_D \sim 3-4$ MHz ($A_H \sim 19-25$ MHz) to an exchangeable deuteron without resolved quadrupole splittings (eq 2). Re-Mims[41] ENDOR spectra of Uf taken with much shorter τ (Figure 5) illustrate that the frequencies of the peaks in Figure 4A are accurately indicated but that the peaks are artificially sharpened by Mims-ENDOR suppression holes (eq 1). The detailed shape of the ^{2}H spectrum of FeFeUf·PO_4 in Figure 4A is somewhat different from that of the other three complexes studied, in part because of severe spin diffusion whose existence is indicated by the absence of Mims suppression holes; relaxation effects also cause the asymmetry between ν_+ and ν_- intensities not seen in the other spectra. Although this causes the intensity of the extreme low-frequency (ν_-) edge of the pattern to become negligibly small, the hyperfine couplings can be calculated from a single branch of the spectrum (eq 2). The ^{2}H intensity in the ν_+ branch clearly extends to ~2 MHz or more, which corresponds to a coupling for **D1** of $A_D \sim 4$ MHz ($A_H \sim 26$ MHz) in this complex as well.

On the basis of its large hyperfine coupling, the deuteron(s) giving rise to this broad signal, designated **D1**, can be assigned to either the hydroxo bridge or a terminal water/hydroxide on the Fe^{3+} of the mixed-valence diiron center.[45,48−50] To distin-

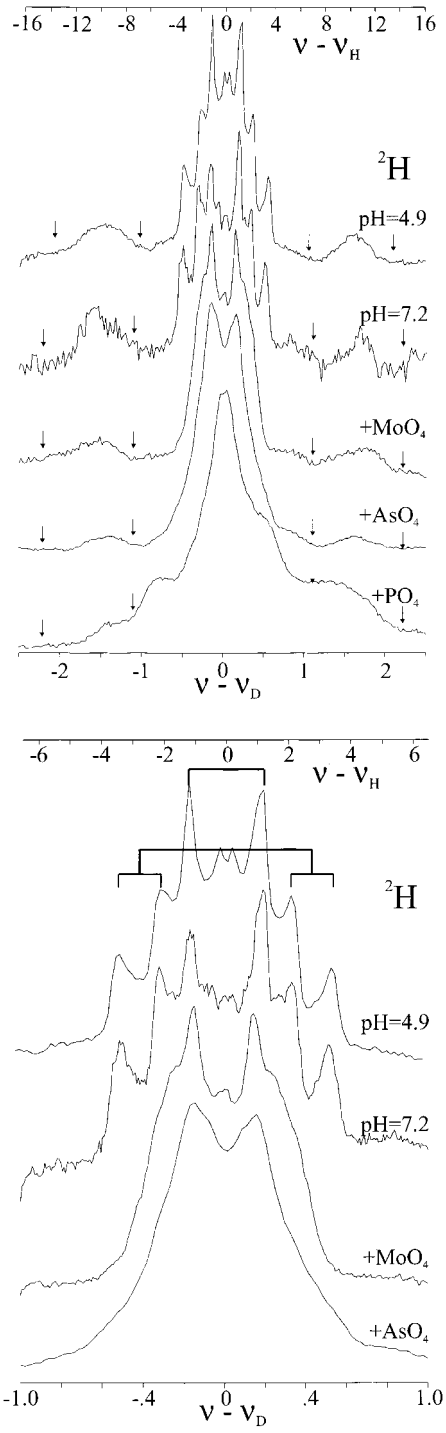

Figure 4. ^{2}H ENDOR spectra at $g_2 = 1.74$ for Uf in D_2O buffer at pD = 4.9 (Uf-pD 4.9) and pD = 7.2 (Uf-pD 7.2), at $g_2 = 1.52$ for the Uf·MoO_4 complex at pD = 4.9, at $g_2 = 1.58$ for the Uf·AsO_4 complex at pD = 4.9, and at $g_2 = 1.51$ for the Uf·PO_4 complex at pD = 4.9. (**A**, **top panel**) Broad sweep. Conditions: Mims three-pulse sequence, pulse lengths t_p = 52 ns; 60 μs Rf pulse between pulses 2 and 3. For Uf-pD 4.9: $\tau = 480$ ns; 34.869 GHz MW frequency, $g = 1.74$; repetition time 15 ms; 60 shots per point per scan; 10 scans. For Uf-pD 7.2: $\tau = 452$ ns; 34.744 GHz MW frequency, $g = 1.74$; repetition time 20 ms; 40 shots per point; five scans; For Uf·MoO_4: $\tau = 452$ ns; 34.701 GHz MW frequency, $g = 1.52$; repetition time 5 ms; 100 shots per point; 30 scans. For Uf·AsO_4: $\tau = 452$ ns; 34.820 GHz MW frequency, $g = 1.58$; repetition time 5 ms; 100 shots per point; eight scans. For Uf·PO_4: $\tau = 452$ ns; 34.760 GHz MW frequency, $g = 1.510$; repetition time 5 ms; 100 shots per point; 23 scans. (**B**, **bottom panel**) Narrow sweep. Conditions were the same as in panel A, except for the number of scans: for Uf-pD 4.9, 10 scans; for Uf-pD 7.2, nine scans; for Uf·MoO_4, 40 scans; for Uf·AsO_4, eight scans.

(47) Doi, K.; McCracken, J.; Peisach, J.; Aisen, P. *J. Biol. Chem.* **1988**, *263*, 5757−5763.
(48) Willems, J.-P.; Lee, H.-I.; Burdi, D.; Doan, P. E.; Stubbe, J.; Hoffman, B. M. *J. Am. Chem. Soc.* **1997**, *119*, 9816−9824.
(49) DeRose, V. J.; Liu, K. E.; Kurtz, D. M., Jr.; Hoffman, B. M.; Lippard, S. J. *J. Am. Chem. Soc.* **1993**, *115*, 6440−6441.
(50) Smoukov, S. K.; Kopp, D. A.; Valentine, A. M.; Davydov, R.; Lippard, S. J.; Hoffman, B. M. *J. Am. Chem. Soc.* **2001** (in press).

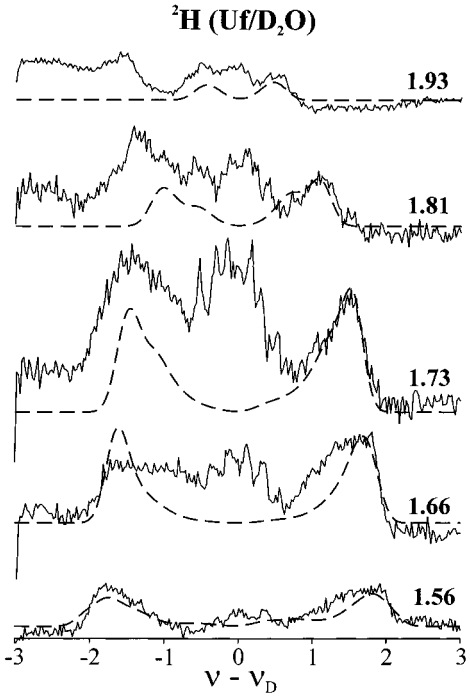

Figure 5. Field-dependent ^{2}H Re-Mims pulsed ENDOR spectra of Uf in D_2O buffer at pH = 4.9. Conditions from top to bottom for all spectra except at $g = 1.58$: 34.804 GHz MW frequency, Re-Mims four-pulse sequence, pulse lengths $t_p = 32$, 32, 32, and 60 ns, with 60 μs Rf pulse between pulses 2 and 3, MW power optimized for a maximum echo with a Mims sequence with 32 ns pulses, $\tau = 164$ ns, repetition time 12 ms, 80 shots per point per scan, 10 scans each. Conditions for spectra at $g = 1.582$: 34.869 GHz MW frequency, Mims three-pulse sequence, $\pi/2$ pulse lengths $t_p = 52$ ns; 60 μs Rf pulse between pulses 2 and 3, $\tau = 480$ ns, repetition time 15 ms, 60 shots per point per scan, two scans; overlaid with a ^{1}H Davies pulsed ENDOR spectrum taken at 9.641 GHz MW frequency, centered at ν_H and scaled by 6.51 to the ^{2}H scale. $\pi/2$ pulse lengths $t_p = 120$, 60, and 120 ns, with 60 μs Rf pulse between pulses 2 and 3, $\tau = 478$ ns, repetition time 12 ms, 86 shots per point per scan, four scans. Simulations: $A = [-3.50, -0.70, +4.20]$ MHz, $\gamma = 90°$, $\beta = 30°$; $P = [-0.035, -0.035, 0.070]$ MHz, $\gamma = 45°$, $\beta = 50°$; hwhm EPR line width = 200 MHz, hwhm ENDOR line width = 0.3 MHz, MW frequency = 34.804 GHz, $\tau = 164$ ns.

guish between these two possibilities, the two-dimensional field-dependent ^{2}H Re-Mims ENDOR patterns for **D1** and **D2** have been collected for Uf (Figure 5) and the Uf·MoO_4 complex (data not shown). The available field (up to $g = 1.5$) encompasses the entirety of the spectra for Uf and most of that for the roughly axial spectrum of the molybdate complex.

The **D1** signal for Uf has its smallest hyperfine coupling at g_1 [$A(g_1) \sim 1$ MHz]; the coupling increases smoothly as the g value of observation is increased, reaching the maximum coupling, $A_{max} \approx 4.2$ MHz, at or near g_3. As shown in Figure 5, the two-dimensional pattern for Uf (pH 4.9) is successfully simulated[48,51,52] with the highly rhombic hyperfine tensor that is characteristic of the proton of a hydroxo bridge that interacts by through-space dipolar coupling with both Fe ions (Table 2). A similar experiment for Uf·MoO_4 indicated that the **D1** tensor was essentially the same as for Uf (not shown). The two-dimensional pattern cannot be simulated with a tensor characteristic of the proton(s) of a terminal aqua ligand to Fe^{3+}, which would have an essentially axial hyperfine tensor, $\mathbf{A} \approx [-T, -T, 2T]$, where $2T \sim 4.2$ MHz.[48] In such a case, the observation of a maximum hyperfine coupling of $A(g_3) \sim 2T \sim 4$ MHz near g_3 would require that the minimum coupling near g_1 have the value $|A(g_1)| \sim T \sim 2$ MHz, significantly larger than observed. In short, the characteristics of the **D1** for Uf and Uf·MoO_4 are those of a hydroxo bridge, not a terminal water/hydroxide. Furthermore, neither Uf (pD = 4.9, 7.2) nor Uf·MoO_4 (pD = 4.9) shows additional ^{2}H intensity with comparable maximum coupling that is unaccounted for by the hydroxo bridge (different field variation), which indicates that there is a hydroxo bridge but no terminal water/hydroxide on Fe^{3+} in these states.[53] The extended breadth of the EPR signals for the arsenate and phosphate complexes, which places much of their EPR envelopes out of range of our magnet, precluded a complete analysis of their **D1** hyperfine tensors. However, given the magnitude of the hyperfine coupling of the **D1** signals in these complexes, they can arise only from a hydroxo bridge or a terminal water/hydroxide on the Fe^{3+}.

Deuterons 2 and 3. In panel A of Figure 4, and its expansion in panel B, the spectra of Uf at both pH values show a second exchangeable proton signal, denoted **D2**, which appears as a doublet of doublets with a hyperfine coupling $A(^2H) \sim 0.85$ MHz [corresponding to $A(^1H) = \sim 5.5$ MHz] and a quadrupole splitting of $|3P| = 0.21$ MHz. This assignment is confirmed in a series of experiments through use of the Mims suppression effect (eq 1): as the value of τ is varied, the two peaks of each doublet are jointly suppressed according to eq 2 (Figure S1 in the Supporting Information), as required for a pair of quadrupole-split doublets separated by $A(^2H)$.

The size of the **D2** hyperfine coupling suggests that this signal should be assigned to a terminal aqua ligand on Fe^{2+}.[50] This is confirmed by the observation, in Figure 4, that the **D2** signal is abolished when molybdate or arsenate binds to form the Uf·MoO_4/AsO_4 complex. Assuming that the conserved protein ligands are unchanged, a bridging tetraoxo anion, as seen crystallographically in the PAP−WO_4 and −PO_4 complexes,[13,16] must displace all the terminal solvent ligands. The spin-relaxation properties of the Uf·PO_4 sample that distorted the **D1** signal have even more deleterious effects on the ability to characterize **D2**; hence Figure 4B does not contain the expansion for Uf·PO_4.

The assignment of the **D2** signal to an Fe^{2+}-bound aqua ligand in Uf is supported by analysis of the two-dimensional field-frequency plot for **D2** (Figure 6). As shown in the figure, the **D2** hyperfine coupling is maximal at $g \sim 1.66$ and gradually decreases toward the high- and low-field edges of the Uf EPR envelope, although the behavior at the low-field edge of the EPR spectrum is unobservable because the **D2** signal becomes overlapped by intensity from **D1**. Simulation of the two-dimensional field-frequency plot with a single deuteron whose hyperfine and quadrupole tensors are $\mathbf{A} = [-0.49, -0.49, 0.98]$ MHz and $\mathbf{P} = [-0.035, -0.035, 0.070]$ MHz[54] gives an excellent fit to experiment (the broad shoulders on each side of the pattern at lower magnetic field are from the strongly coupled **D1** signal) (Figure 6 and Figure 5). The **D2** hyperfine tensor components have the values expected for a terminal solvent-

(51) DeRose, V. J.; Hoffman, B. M. In *Methods in Enzymology*; Sauer, K., Ed.; Academic Press: New York, 1995; Vol. 246, pp 554−589.
(52) Hoffman, B. M.; Gurbiel, R. J.; Werst, M. M.; Sivaraja, M. In *Advanced EPR. Applications in Biology and Biochemistry*; Hoff, A. J., Ed.; Elsevier: Amsterdam, 1989; pp 541−591.
(53) Note also that the pattern for the axial tensor of a terminal solvent proton is typically more intense than that for the fully rhombic tensor of the bridge.
(54) The tensors are noncoaxial with the **g** tensor and with each other; the orientation parameters are given in the caption to Figure 4.

Table 2. **A** Tensors for Water-Derived Ligands Bound to the Fe^{3+} in Mixed-Valence Diiron Proteins

protein system	principal values (MHz)	Euler angles[a] (deg)	assignment
$MMOH_{mv}$	[−25, −5, +30]	$\alpha = 0; \beta = 45$	hydroxo bridge[45]
RNR R2 X-intermediate	[−10.25, −10.25, 20.5]	$\alpha = 10; \beta = 73$	Fe^{3+} terminal water (two protons)[48]
	[−8.8, −8.8, 17.6]	$\alpha = 20; \beta = 90$	
$Fe^{3+}Fe^{2+}$Uf	[−22.5, −4.5, +27][b]	$\alpha = 90; \beta = 30$	hydroxo bridge (this work)

[a] Euler angles defined as previously.[43,51] [b] For ^{2}H the values are [−3.5, −0.7, 4.2].

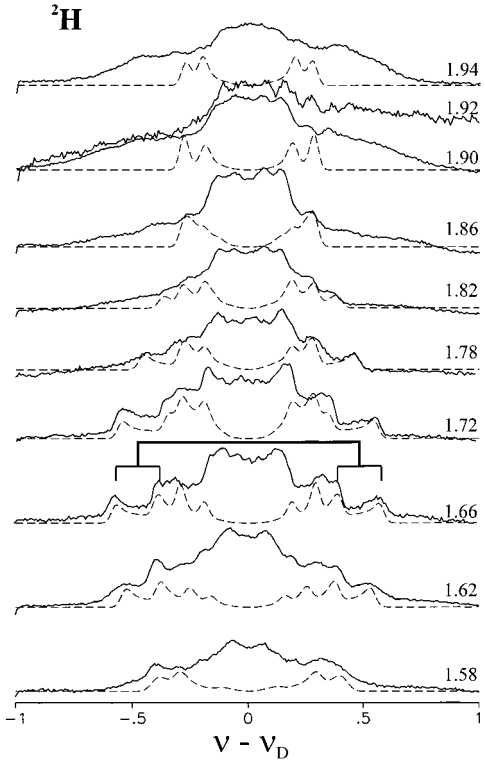

Figure 6. Field-dependent ^{2}H Mims pulsed ENDOR spectra of Uf in D_2O buffer at pH = 4.9 of the weakly coupled ^{2}H signal. Two different kinds of conditions were used: for spectra marked with an asterisk, 34.853 GHz MW frequency, Mims three-pulse sequence, $\pi/2$ pulse lengths $t_p = 52$ ns; 20 μs Rf pulse between pulses 2 and 3, repetition time 20 ms, 30 shots per point per scan; and for spectra marked with a dagger, 34.869 GHz MW frequency, Mims three-pulse sequence, $\pi/2$ pulse lengths $t_p = 52$ ns; 60 μs Rf pulse between pulses 2 and 3, $\tau = 480$ ns, repetition time 15 ms, 60 shots per point per scan. *($g = 1.940$) 10 scans; †($g = 1.916$) eight scans; *($g = 1.900$) 10 scans; *($g = 1.860$) four scans; *($g = 1.820$) four scans; †($g = 1.780$) four scans; †($g = 1.718$) six scans; †($g = 1.661$) seven scans; *($g = 1.620$) 10 scans; *($g = 1.580$) four scans. Simulations: $A = [-0.049, -0.049, 0.098]$ MHz, $\gamma = 65°$, $\beta = 44°$; $P = [-0.035, -0.035, 0.070]$ MHz, $\gamma = 45°$, $\beta = 50°$; hwhm EPR line width = 200 MHz, hwhm ENDOR line width = 0.04 MHz, MW frequency = 34.869 GHz, $\tau = 480$ ns.

derived aqua ligand bound to the Fe^{2+} ion at a normal Fe−O bond length.[50]

The spectroscopic signatures of both the bridge (**D1**) and the aqua ligand (**D2**) of Uf are unchanged upon raising the pD from 4.9 and 7 (Figure 4), indicating that there is no change in the protonation states of these ligands over this pH range. The terminal solvent ligand on the Fe^{2+} ion of Uf thus is likely a water, which is expected to have a pK_a of $\sim$ 9.5.[55]

Finally, the sharp peaks at ±0.18 MHz in the top three spectra of Figure 4B are assigned to a third exchangeable site, **D3**, which has a hyperfine coupling $A(^2H) \sim 0.37$ MHz [$A(^1H) = \sim 2.4$ MHz] at the fields of observation; this signal is not present in the Uf·AsO_4/PO_4. The coupling for this site is too small to be associated with a proton from a solvent-derived ligand to iron and may reflect an H-bond; this signal is not discussed further.[56]

Discussion

The present ENDOR study of Uf and the Uf·MoO_4/AsO_4/PO_4 complexes shows that the Fe^{3+}/Fe^{2+} mixed-valence diiron center of Uf in solution has *only* two solvent-derived ligands at pH 5 and at pH 7. One has a strongly coupled proton (**D1**), with maximum coupling of $A_H \sim 25$ MHz; this signal persists in the anion complexes. Comparison with the data for related complexes (Table 2) shows that such a large coupling constant can only be assigned to either a hydroxo bridge or a terminal water/hydroxide on Fe^{3+}. The field dependence of the **D1** signal for Uf and the Uf·MoO_4 complex strongly supports its assignment to the hydroxo bridge. This assignment is confirmed by the very observation that the two-dimensional signal pattern persists after binding of MoO_4. X-ray diffraction and EXAFS studies of complexes of PAPs with all the tetraoxo anions considered here, MoO_4/AsO_4/PO_4, indicate that all these ligands bind to the dinuclear center in a bidentate bridging mode, occupying the two axial coordination sites available for solvent binding.[13,16,35,36] Thus, the only strongly coupled, exchangeable proton that *could* remain in the tetraoxo anion complexes is that of the hydroxo bridge. The magnitude of the **D1** coupling for the analogous Uf·AsO_4/PO_4 is consistent with this picture.

The second, more weakly coupled exchangeable proton seen for Uf (**D2**) is assigned to a terminal water/hydroxide coordinated to the Fe^{2+} ion, in part because it is lost upon MoO_4/AsO_4 binding. The pK_a of a water molecule bound to either Fe^{2+} or Zn^{2+} is expected to fall between 9 and 10,[55] while the data show that the protonation states of the bridge and the terminal aqua ligand are unaltered by an increase in pD from 4.9 to 7.0, in accordance with assignment to a bound water. This also parallels the assignment of a water ligand to the Zn^{2+} center of the PAP from kidney beans, based on the observation of a pH transition with a pK_a of 9.5.[13] Such an assignment does, however, make the observation of such sharp features somewhat surprising, as they would presumably come from two deuterons that are very well ordered (therefore the sharp peaks) and accidentally equivalent.

Most significantly, there is no signal that can be attributed to a terminal water or hydroxide bound to the Fe^{3+} ion of Uf (or for a tetraoxo anion complex, as represented by Uf·MoO_4). This observation suggests that the sixth coordination site on the Fe^{3+} ion of mixed-valence Uf is vacant. This conclusion would contradict the central tenet of the proposed mechanism shown in Figure 2 involving a terminal hydroxide nucleophile in phosphate ester hydrolysis. According to this mechanism,

(55) Baes, C. F.; Mesmer, E. *The Hydrolysis of Cations*; Wiley-Interscience: New York, 1986; pp 226−237.

(56) This coupling not only seems too small to be the second proton from the terminal water in Uf but also does not appear to be lost in the molybdate complex.

favored by a number of groups,[13,27,30] the sixth site on the Fe^{3+} ion harbors a terminal hydroxide, which would act either directly as the nucleophile required for substrate hydrolysis or as a base to generate the active nucleophile from a nearby noncoordinated water molecule. This notion derives from the observed pK_a of 3.5−5 for the pH dependence of enzymatic activity, EPR spectra, and rates of phosphate binding to Uf and BSPAP.[27,29−31] The observed pK_a is certainly within the range for the deprotonation of a water molecule coordinated to a Fe^{3+} ion.[55] In support, the recent X-ray structure of a mammalian PAP in the sulfate-bound diferric form shows a terminal water/hydroxide ligand coordinated to the tyrosinate-bound Fe^{3+} ion.[15] However, this structure does not represent the active form of the enzyme and the observed terminal water/hydroxide may be a specific feature of this diferric form. In addition, this structure shows the presence of a third metal ion, Zn^{2+}, in the active site, originating from the high concentration of $ZnCl_2$ used in the crystallization buffer. The perturbation caused by this cation on the hydration of the active site may limit the usefulness of this structure in the identification of water ligands in the active site. Indeed no solvent-derived ligand can be discerned from the only X-ray structure of an active PAP.[12]

The apparent absence of a terminal solvent ligand on the Fe^{3+} ion of Uf, which casts doubt on the terminal hydroxide nucleophile mechanism (Figure 2, mechanism A), leads us to further scrutinize the bridging hydroxide nucleophile mechanism (Figure 2, mechanism B). This hypothesis is disfavored by the likelihood that a hydroxide which bridges two Lewis-acidic metal centers would be a poorer nucleophile than its terminally coordinated counterpart.[13] However, the reduced nucleophilicity of the bridging hydroxo ligand can be compensated by an increased electrophilicity of the bridging substrate, which undergoes double Lewis acid activation when acting as a bridge to the dimetal site[57] (Figure 2). The substrate in mechanism B (Figure 2) would thus be more activated than that in mechanism A, where the phosphate group must be terminally coordinated to the divalent metal ion.

Diminution of the nucleophilicity of the hydroxo bridge also could be counteracted by the following effect. The binding of phosphate ion to the $Fe^{3+}Fe^{2+}$ form of the enzyme has been shown to decrease the coupling interaction between the two metal centers, as indicated by a decrease in J from 20 to 6 cm^{-1}.[20] Corresponding magnetic circular dichroic (MCD) data suggest that this weakening of the antiferromagnetic interaction may arise from a shift of the hydroxo bridge away from the trivalent ion and toward the divalent cation.[22] Such a shift would effectively increase the nucleophilicity of the bridge toward the incoming substrate.

Our conclusions regarding the solvent-derived ligands of Uf must be tempered by the crystallographic results for calcineurin, a phosphatase with an $Fe^{3+}-Zn^{2+}$ site very similar to that of the PAPs but with a pH optimum at neutral pH.[10] However, unlike in the PAPs, the trivalent site of calcineurin is six-coordinate with two terminal solvent ligands in place of the characteristic tyrosinate ligand found in PAPs. For this enzyme it is not possible to exclude either of the two possible mechanisms by arguments based on the coordination sphere of the metals. If Uf and calcineurin were to share the same hydrolytic mechanism, our data would require that both enzymes operate via mechanism B.

A consideration of the structure of the enzyme−substrate complex also can be useful for discriminating between mechanisms A and B. Mechanism A requires the phosphate ester substrate to bind as a monodentate ligand on the Fe^{2+} ion, while mechanism B postulates the binding of the phosphate ester substrate as a bidentate bridge. To date, there is no conclusive experimental evidence that establishes the structure of the enzyme−substrate complex. In rapid freeze−quench EPR studies of the bovine spleen PAP,[27] Merkx et al. have observed two spectroscopically distinct forms of the phosphate and substrate complexes, which they interpret as arising from a bridging and a terminal coordination geometry of the phosphate group. In their proposal only the conformation with a terminal geometry is active in substrate hydrolysis; unfortunately, more definitive structural evidence on the character of these intermediates is not yet available. On the other hand, EXAFS studies of a ternary FeZnUf·PO_4·F complex, which is proposed to model FeZnUf·O_3P(OR)·OH, the putative activated enzyme−substrate complex, supported a bidentate phosphate bridge.[35] This geometry is similar to the one observed for the binding of inorganic phosphate, giving rise to the notion that the Uf·PO_4 complex may serve as a good model for the enzyme−substrate complex. The possibility that Uf·PO_4 represents a catalytically competent species is supported by the observation that Uf can catalyze ^{18}O exchange of phosphate ion itself with $H_2{}^{18}O$.[58]

Examination of the active-site structures of PAPs can provide some insight into the possible geometry of substrate binding. The structures display a broad but shallow channel leading toward the dinuclear center from a direction perpendicular to the plane of the bridged core; this cavity has been proposed to be the substrate access channel.[13,15,16] It is likely that a substrate would enter the channel with its negatively charged PO_3 group pointed toward the positively charged dinuclear center and its bulkier leaving group oriented toward the open end of the channel. This would allow the phosphate ester to bind in a bridging mode with very few constraints, as postulated in mechanism B (Figure 2). In this mechanism, the axis of in-line attack by the hydroxo bridge is perpendicular to the metal−metal axis; the alcoholate leaving group would be optimally oriented along the axis of the access channel, and its egress during turnover would be unimpeded. On the other hand, mechanism A requires some reorganization of the active site, since the axis of in-line attack of the terminal hydroxide would be parallel to the metal−metal axis (Figure 2) and the alcoholate leaving group would have to be placed in a region already occupied by several amino acid residues. These considerations also lead us to favor mechanism B.

To date, a hydrolytic mechanism such as B, involving a hydroxo bridge, has been proposed for several dinuclear hydrolases possessing a variety of metal centers. Evidence is mostly derived from crystallographic studies of the enzymes and their complexes with inhibitors believed to be transition-state analogues. Among these enzymes, arginase, with a dimanganese(II) active site, provides the strongest case in favor of a bridging nucleophile.[2,59−61] Contrary to what is required

(57) Wall, M.; Hynes, R. C.; Chin, J. *Angew. Chem.* **1993**, *105*, 1696−1697. See also *Angew. Chem., Int. Ed. Engl.* **1993**, 1632 (1611) and 1633−1635.

(58) Wynne, C. J.; Hamilton, S. E.; Dionysius, D. A.; Beck, J. L.; de Jersey, J. *Arch. Biochem. Biophys.* **1995**, *319*, 133−141.

(59) Cox, J. D.; Kim, N. N.; Traish, A. M.; Christianson, D. W. *Nat. Struct. Biol.* **1999**, *6*, 1043−1047.

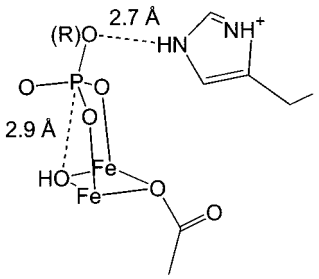

Figure 7. Structure of the $Fe^{3+}Fe^{3+}$Uf-PO_4 complex, extracted from PDB file 1ute, showing the orientation of the bound phosphate and bridging hydroxide.

for hydrolysis of most biological substrates, hydrolysis of the positively charged guanidinium group of arginine does not need substrate activation by coordination to a metal center. A hydroxo bridge constitutes the only water-derived ligand of the dinuclear cluster and the only available nucleophile. Its involvement in catalysis is further supported by the complex with the inhibitor 2(*S*)-amino-6-boronohexanoic acid.[59] In this structure the hydroxyl group of the ligand acts as the bridge, replacing the hydroxide ion observed in the resting form. Such a structure has been proposed to mimic the geometry of the transition state arising from the formation of a covalent bond between substrate and nucleophile. Therefore, coordination of the hydroxide to the bridging site is taken as strong evidence that the nucleophile required for hydrolysis originates from that same position.

A similar conclusion has been drawn by comparing the structure of dicobalt(II) methionine aminopeptidase with those of its complexes with bestatin- and phosphonate-based inhibitors.[7,62] In the structure of the as-isolated enzyme, the dinuclear site has two solvent-derived ligands, a bridging hydroxide and a terminal ligand on one of the Co(II) centers, with the other Co(II) center having a vacant terminal coordination site, similar to what we have deduced for Uf. The binding of bestatin or phosphonic acids, which are believed to be analogues of the tetrahedral transition state, results in the replacement of the bridging hydroxide by a hydroxyl of the inhibitor.

Proximity and the relative orientation of nucleophile and electrophile are also important factors that control reactivity. The crystal structures of the phosphate complexes of both FeZn KBPAP and diferric uteroferrin[13,16] show that phosphate ion binding to the dimetal core is not symmetric relative to the metal−metal axis and is in fact tilted toward the bridging hydroxide side of the planar $Fe(O)_2Fe$ rhombohedron (Figure 7). As a consequence, the hydroxo bridge, the phosphorus atom, and one oxygen atom of the phosphate anion (which would be part of the leaving group in the substrate complex) all lie in a straight line and are set up for in-line displacement. The tilted orientation appears to be induced by interaction of the phosphate with residues in the active site, so as to facilitate the formation of the pentavalent phosphorus intermediate. This is in accordance with the view that the enzyme active site stabilizes the transition state formed by reaction of the Michaelis complex.

According to this model, release of the leaving group would produce a complex with the phosphate product bound as a tridentate ligand, occupying the two terminal coordination sites and acting as a bridge. The geometry of such a complex is different from that of the crystallized uteroferrin/phosphate complex and is expected to be thermodynamically less stable due to the strained coordination of the two terminally bound oxygen atoms of phosphate. However, the recent crystal structures of a dimanganese(II) phosphatase complexed with the inhibitor sulfate[17] and the dinickel(II) urease complexed with the inhibitor phosphate[63] demonstrate that such tridentate binding mode for a tetraoxo anion can be achieved in related active sites.

Conclusions

This study allows us to discriminate between the two proposed mechanisms for PAP catalysis, one that favors a terminal hydroxide as the nucleophile[13,27,29] and another that favors the hydroxo bridge.[32] The ^{2}H Q-band pulsed ENDOR measurements reported here indicate that the active $Fe^{3+}Fe^{2+}$ form of Uf contains a terminal water/hydroxide bound to Fe^{2+} and a hydroxo bridge but no terminal water/hydroxide bound to Fe^{3+}. The Uf·MoO_4 anion complex retains the hydroxo bridge but has no terminal water ligands, in particular no terminal water/hydroxide bound to Fe^{3+}, and it is argued that the same is true for the corresponding AsO_4/PO_4 complexes. These results favor a mechanism that relies on the bridging hydroxide as the nucleophile (Figure 2, mechanism B). Since our conclusion is based on what we have learned about the structure of the as-isolated active enzyme, we cannot exclude the possibility that the coordination environment of the dinuclear center could change significantly upon substrate binding, generating the putative terminal hydroxide nucleophile. Nevertheless, the ENDOR evidence and other arguments raised in the previous section now make mechanism B the more likely mechanism for PAP hydrolysis The assignment here of a catalytic role for the bridging hydroxide of the PAPs, in addition to its structural role, is in consonance with prevailing mechanisms for other evolutionarily unrelated metallohydrolases with hydroxo-bridged dimetallic active sites.[1]

Acknowledgment. We acknowledge Dr. Jean-Paul Willems for early spectroscopic studies and Mr. Clark E. Davoust for superb technical support. This work was supported by grants from the National Science Foundation (DMB9808350 to L.Q. and DMB-9904018 to B.M.H.) and the National Institutes of Health (HL 13531 to B.M.H.).

Supporting Information Available: One figure showing τ-dependent ^{2}H Mims pulsed ENDOR spectra of Uf. This information is available free of charge via the Internet at http://pubs.acs.org.

JA003169L

(60) Cox, J. D.; Cama, E.; Colleluori, D. M.; Pethe, S.; Boucher, J.-L.; Mansuy, D.; Ash, D. E.; Christianson, D. W. *Biochemistry* **2001**, *40*, 2689−2701.
(61) Kim, N. N.; Cox, J. D.; Baggio, R. F.; Emig, F. A.; Mistry, S. K.; Harper, S. L.; Speicher, D. W.; Morris, S. M., Jr.; Ash, D. E.; Traish, A.; Christianson, D. W. *Biochemistry* **2001**, *40*, 2678−2688.
(62) Lowther, W. T.; Zhang, Y.; Sampson, P. B.; Honek, J. F.; Matthews, B. W. *Biochemistry* **1999**, *38*, 14810−14819.
(63) Benini, S.; Rypniewski, W. R.; Wilson, K. S.; Ciurli, S.; Mangani, S. *JBIC* **2001**, *6*, 778−790.